CHAPTER III

OPTICAL BISTABILITY IN PERIODIC STRUCTURES

A. Introduction

Periodic structures play a rather fundamental role in optics. The diffraction grating of classical optics utilizes the wavelength selective reflection and transmission properties of periodic structures to perform spectral analysis. In the modern field of integrated optics periodic thin film dielectric waveguides are used as filters, input and output couplers and as "mirrors" in distributed Bragg reflector (DBR) and distributed feedback (DFB) lasers [1]. Distributed feedback structures are compact, possess a high degree of spectral selectivity and are compatible with the planar technology of integrated optics.

Recently, Okuda et al. [2] have considered the use of Bragg reflectors as mirrors for a bistable optical device. Although that device employs periodic structures, conceptually it is not much different from the Fabry Perot type since they both depend on a feedback mechanism localized at the ends of a homogeneous nonlinear medium. Subsequently, we proposed and presented an exact analysis of a new device concept in which the feedback mechanism is distributed throughout and integrated within the nonlinear medium as a

periodic perturbation of the refractive index [3]. On the theoretical side, the discovery of closed form solutions for this problem of nonlinear interactions in a periodic structure is a significant advance. (The closely related problem of gain saturation in DFB lasers has resisted attempts at exact solution for a decade [4].) In this chapter we present a more detailed description of the distributed feedback bistable optical device. We consider the effects of a saturable nonlinear index, of loss, chirp and taper, and conclude with design considerations for a practical device that may be built using the concepts discussed here.

B. Simple Model of Bistability in a DFB Structure

Before we begin the analysis we review some of the properties of a linear grating and present a simple physical picture of bistability in a nonlinear DFB structure.

The grating structures under consideration are shown in Figs. (3.1a) and (3.1b). They may be waveguides with a periodic corrugation of their boundaries or bulk media with a periodic perturbation in the dielectric constant. A light wave will interact strongly with these structures if the period of the perturbations is an integer multiple of half the light wavelength in the medium. Under this condition (known as the Bragg condition), there is coherent backscattering of a forward-going wave, and the grating acts as a band-rejection filter whose fractional bandwidth in wave-

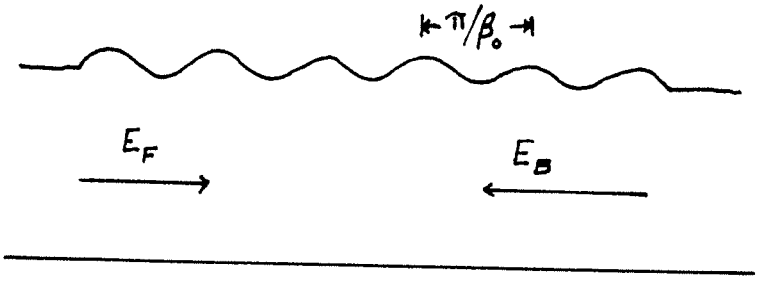

Fig. (3.1a): Waveguide with a periodic surface corrugation.

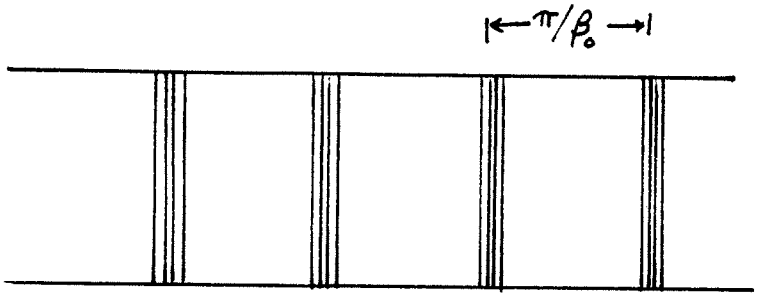

Fig. (3.1b): Thin film with a periodic perturbation of the dielectric constant.

length λ can be shown to be [5]

$$\Delta\lambda/\lambda \simeq \Lambda/L, \tag{3.1}$$

where Λ is the period of the perturbations and L is the length of the structure. The center of this band is at the Bragg wavelength

$$\lambda_0 = 2n\Lambda, \tag{3.2}$$

where n is the refractive index of the bulk medium, or the effective index of the waveguide.

The coupled-wave theory of Kogelnik [5] assumes that only two counterpropagating waves of complex amplitude E_F and E_B exist within the structure. These waves exchange energy as a result of scattering by the index perturbations. The strength of this interaction is measured by a coupling constant κ which is related to the amplitude of the perturbations. The two waves satisfy the coupled-wave equations

$$E_F' = i\kappa E_B \exp(-i2\Delta\beta z) \tag{3.3a}$$

$$E_B' = -i\kappa E_F \exp(i2\Delta\beta z), \tag{3.3b}$$

where primes denote d/dz, and the detuning of the incident light wavelength from the Bragg wavelength is measured by

$$\Delta\beta = \beta - \beta_0 , \tag{3.4}$$

with $\beta = 2\pi n/\lambda$ and $\beta_0 = 2\pi n/\lambda_0$. We remark that for a

corrugated waveguide E_F and E_B represent mode amplitudes in the unperturbed guide. It can be shown [6] that both surface corrugations and bulk index perturbations lead to the same coupled wave equations with the appropriate expressions for the coupling constant κ. The solutions of Eqs. (3.3) with boundary conditions $E_F(0) = 1$ and $E_B(L) = 0$ are

$$E_B(z) = \frac{i\kappa \exp(-i\Delta\beta z)\ \sinh[D(z-L)]}{-\Delta\beta \sinh(DL) + iD\cosh(DL)} \tag{3.5a}$$

and

$$E_F(z) = \frac{\exp(i\Delta\beta z)\cdot\{\Delta\beta \sinh[D(z-L)] + iD\cosh[D(z-L)]\}}{-\Delta\beta \sinh(DL) + iD\cosh(DL)} \tag{3.5b}$$

where

$$D = [\kappa^2 - (\Delta\beta)^2]^{1/2}. \tag{3.6}$$

Under phase-matched conditions ($\Delta\beta = 0$), the power in the forward and backward waves is given by

$$|E_B(z)|^2 = \frac{\sinh^2[\kappa(z-L)]}{\cosh^2(\kappa L)} \tag{3.7a}$$

$$|E_F(z)|^2 = \frac{\cosh^2[\kappa(z-L)]}{\cosh^2 \kappa L}\ . \tag{3.7b}$$

The reflectivity as a function of detuning is found from Eqs. (3.5) to be

$$R = |E_B(0)|^2/|E_F(0)|^2 = \frac{(\kappa L)^2}{(\Delta\beta L)^2 + (DL)^2 \coth^2(DL)}. \tag{3.8}$$

For zero detuning this reduces to

$$R = \tanh^2(\kappa L) \ . \tag{3.9}$$

To complete this review of the properties of the linear grating, we plot the main results (Eqs. (3.5)-(3.9)) in Figs. (3.2)-(3.5). In Fig. (3.2) we show the power in the forward and backward waves as a function of the normalized distance z/L within the grating when $\Delta\beta = 0$. It can be seen that for large coupling constants ($\kappa L > 2$) the field in the structure drops off rapidly within the first few grating periods. Most of the incident light is reflected. Fig. (3.3) shows the reflectivity and transmissivity of the grating as a function of the detuning $\Delta\beta L$ for different values of κL. The width of the central lobe increases with increasing κL and larger sidelobes begin to appear. Finally, Fig. (3.4) shows the reflectivity as a function of κL for zero detuning. Note the rapid increase in R as the coupling constant is increased.

To understand bistability in periodic structures, suppose now that the DFB structure has an intensity-dependent refractive index. Suppose also that the incident light frequency satisfies the Bragg condition for the structure so that at low input intensity most of the light is reflected. As the intensity is increased, more light enters the structure and the change in index due to this light detunes the grating from the incident wavelength. This in turn allows

Fig. (3.2): Distribution of forward and backward fluxes in a grating structure for zero detuning. (a) $\kappa L = 1$, (b) $\kappa L = 2$, (c) $\kappa L = 4$.

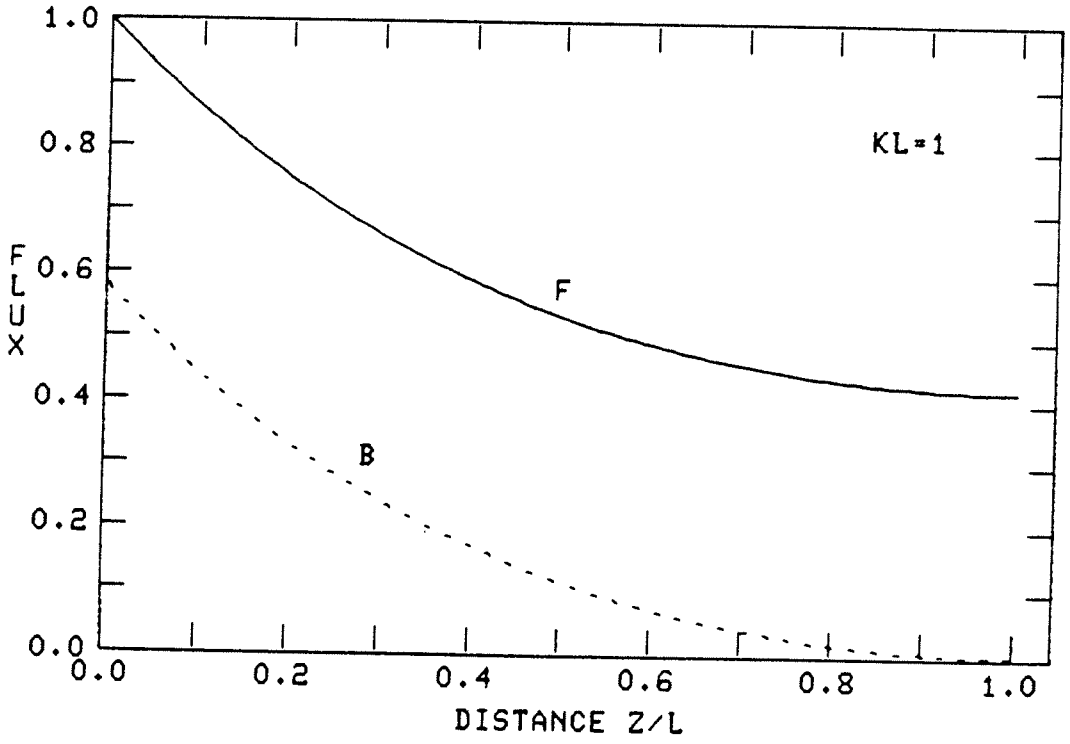

Fig. (3.2a)

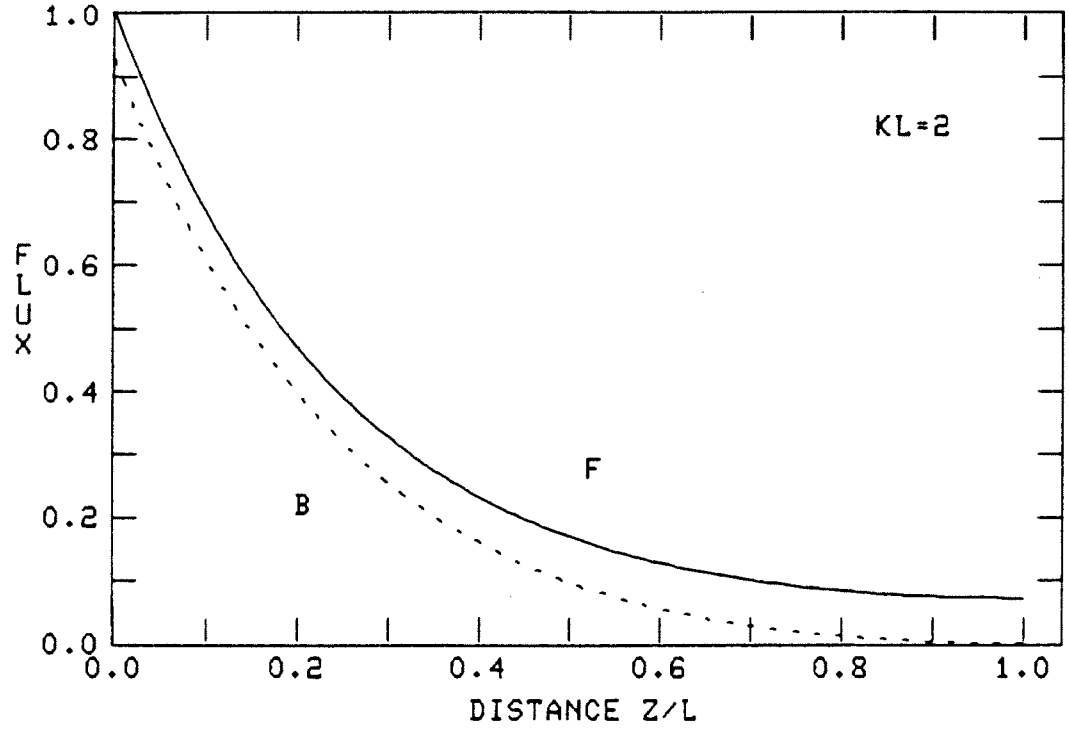

Fig. (3.2b)

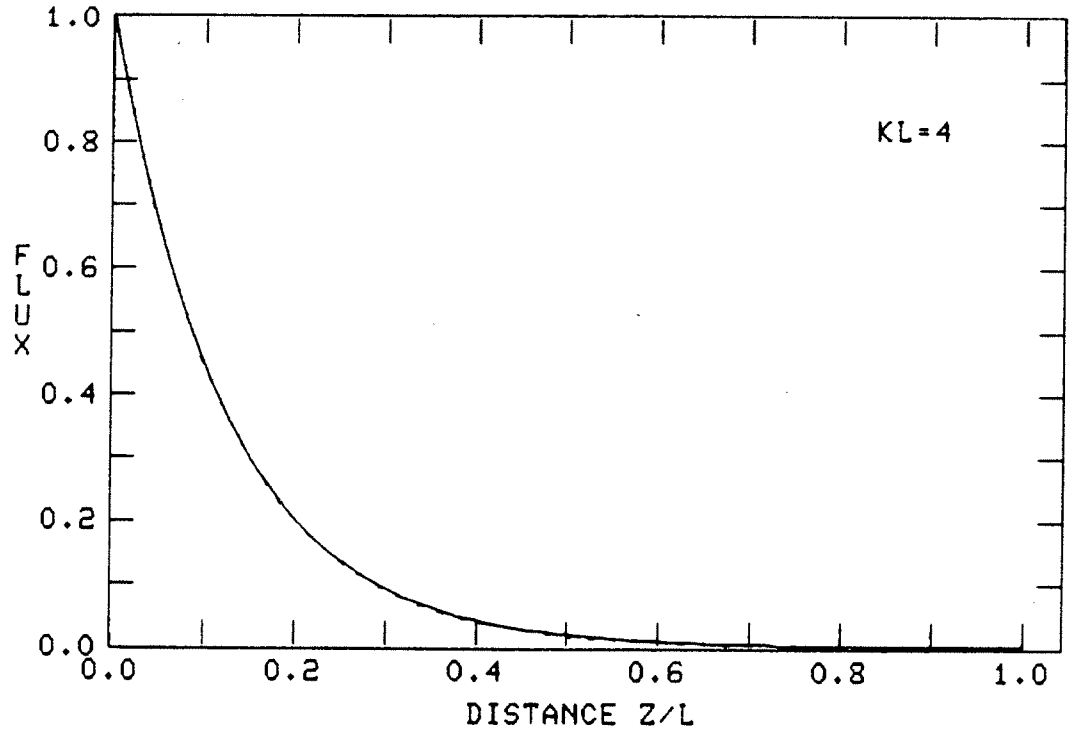

Fig. (3.2c)

Fig. (3.3): Reflectivity (——) and transmissivity (---) of a distributed feedback structure as a function of detuning $\Delta\beta L$ for different values of κL.

(a) $\kappa L = 1$ (b) $\kappa L = 2$ (c) $\kappa L = 4$.

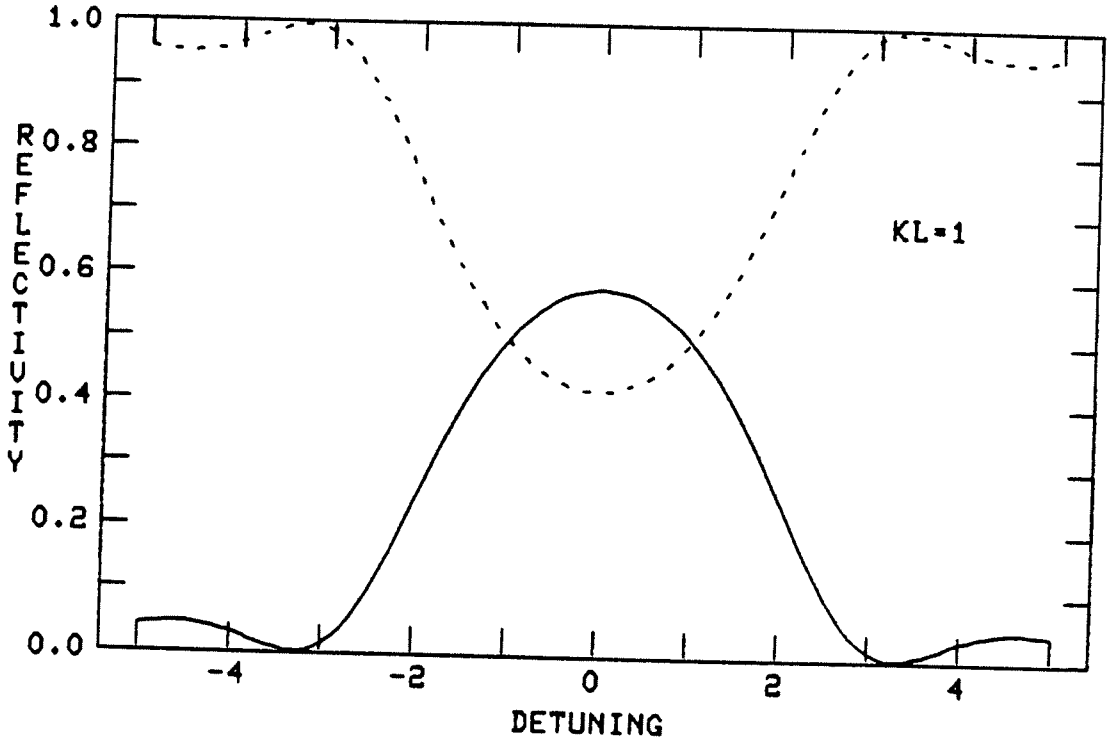

Fig. (3.3a)

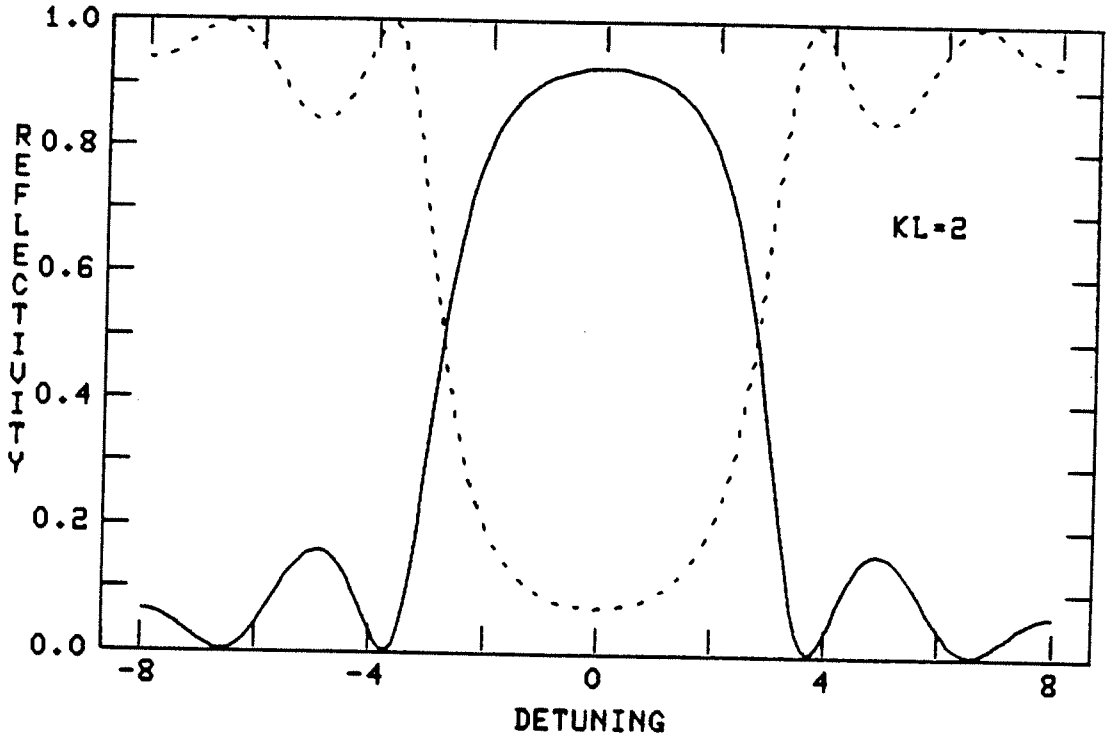

Fig. (3.3b)

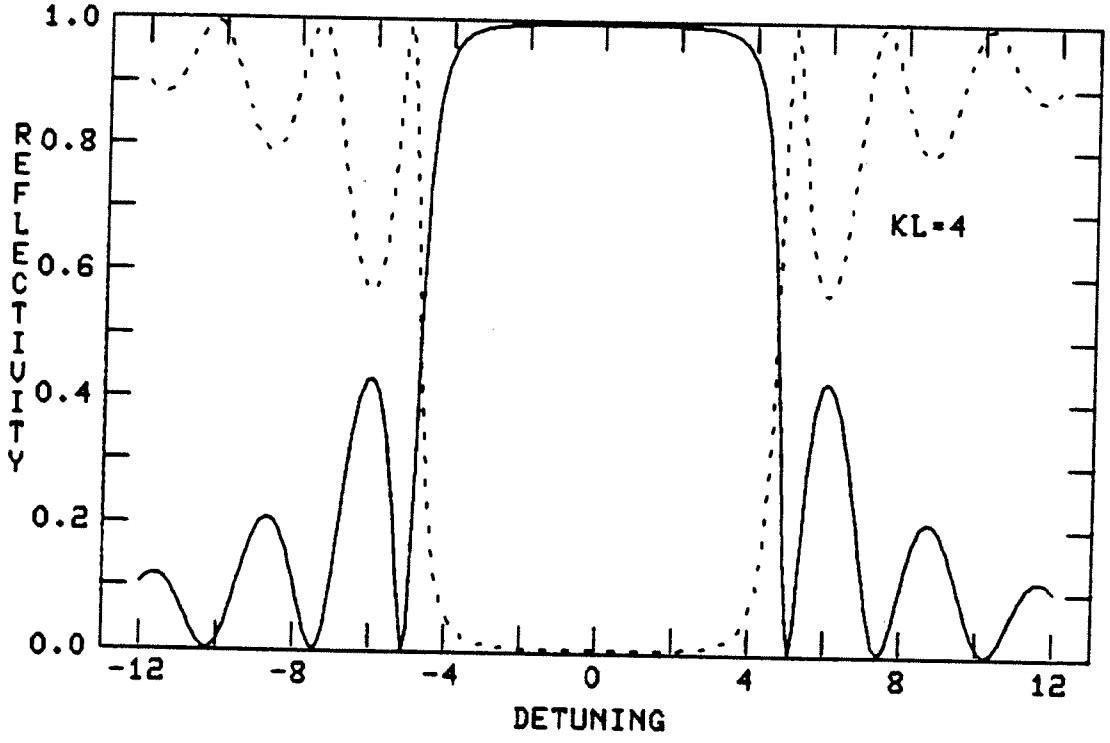

Fig. (3.3c)

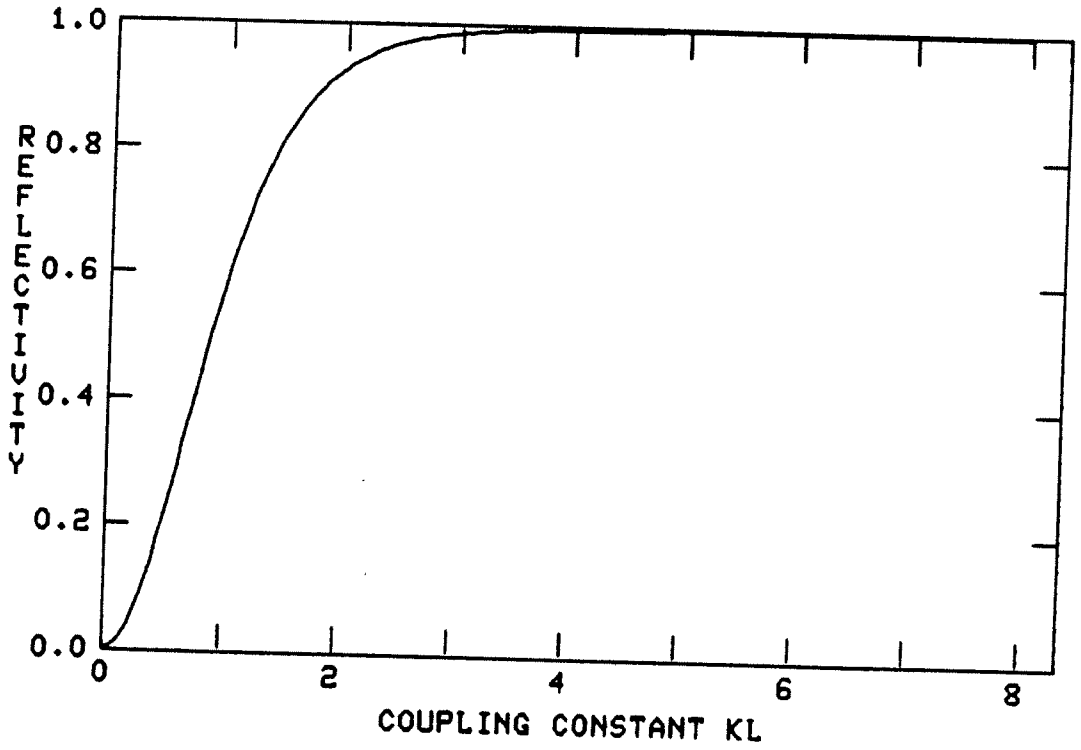

Fig. (3.4): Reflectivity of a distributed feedback structure vs. κL for zero detuning.

more light to enter, until eventually the structure is so detuned that the light wavelength in the nonlinear medium no longer lies within the stopband. The device thus turns on to a high transmission state. As the input intensity is reduced there is still enough light within the structure to keep its index high and maintain it in a high transmission mode. Switch-down to a low transmission state occurs at a lower input intensity than that at which switch-up occurred, resulting in a hysteresis loop. This behavior is illustrated in Fig. (3.5a), which shows the transmission of a nonlinear DFB as a function of input intensity. This curve was generated from an exact solution of the nonlinear coupled-wave equations which we derive in the next section. Also shown in Fig. (3.5b) is the transmission of a linear DFB as a function of detuning. A comparison of Figs. (3.5a) and (3.5b) shows clearly the role of the light intensity as a detuning parameter in the nonlinear DFB structure.

C. The Nonlinear Coupled-Wave Equations

The starting point of the analysis is Maxwell's wave equation for the transverse field E:

$$c^2 \partial_z^2 E = \partial_t^2 (E+4\pi P) \ , \qquad (3.10)$$

where P is the polarization density. We assume that the medium is lossless, the waves are monochromatic and of radian frequency ω, and that no higher harmonics of the incident

Fig. (3.5): The role of input intensity as a detuning parameter in a nonlinear DFB structure.

(a) Transmission of a nonlinear DFB as a function of input intensity.

(b) For comparison, the transmission of a linear DFB as a function of detuning.

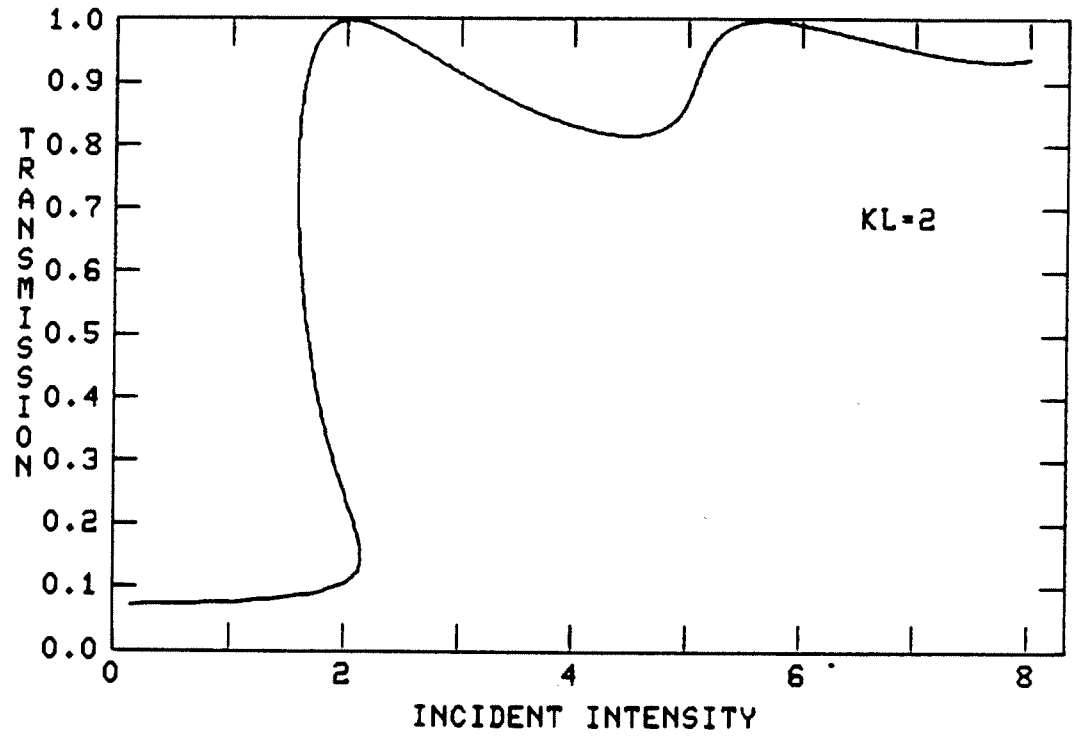

Fig. (3.5a)

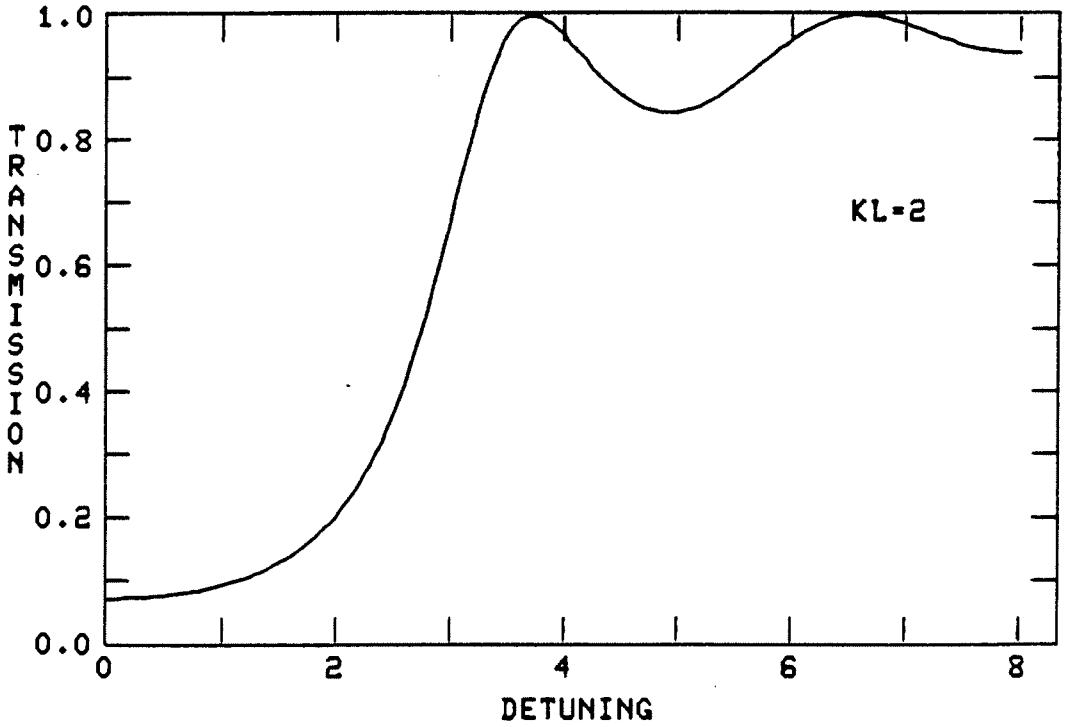

Fig. (3.5b)

wave are generated. In the notation of Maker and Terhune [7], the envelope of the polarization wave can be written

$$P_i = \chi^{(1)}_{ij}(\omega)E_j + 3\chi^{(3)}_{ijkl}(\omega;-\omega,\omega,\omega)E^*_j E_k E_l \ , \qquad (3.11)$$

where $\chi^{(3)}_{ijkl}$ is a component of the fourth rank third order susceptibility tensor. (This well-known formalism for the nonlinear polarization is reviewed in Appendix A.) The complex field envelopes E and P are related to the real fields by

$$\mathbf{E} = \mathrm{Re}Ee^{-i\omega t} \qquad \mathbf{P} = \mathrm{Re}Pe^{-i\omega t} \ . \qquad (3.12)$$

For an isotropic medium and linearly polarized fields the polarization density becomes

$$P = (n^2-1)E/4\pi + 3\chi^{(3)}_{1111}|E|^2E \qquad (3.13)$$

where the periodically modulated refractive index is given by

$$n(z) = n_0 + n_1\cos 2\beta_0 z \ , \qquad (3.14)$$

with $n_1 << n_0$. Using Eqs. (3.14), (3.13) and (3.12) in (3.10) we obtain a form of Matthieu's equation with a nonlinear driving term:

$$\partial_z^2 E + \left(\left(\frac{n_0\omega}{c}\right)^2 + \frac{2n_0n_1\omega^2}{c^2}\cos 2\beta_0 z\right)E = \frac{-12\pi\omega^2}{c^2}\chi^{(3)}|E|^2E \ . \qquad (3.15)$$

We now define the wavenumber $\beta = n_0\omega/c = 2\pi n_0/\lambda$ where λ is the vacuum wavelength of the light. We also recall the Bragg wavelength λ_0 as the wavelength of light which satisfies the Bragg condition $\beta = \beta_0$ for the structure. Following Kogelnik and Shank [5] we introduce a coupling constant

$$\kappa = \frac{\pi n_1}{\lambda_0} \tag{3.16}$$

which measures the strength of feedback per unit length provided by the structure. The effect of the nonlinearity is measured by a constant

$$\gamma = \frac{\pi n_2}{\lambda_0} \tag{3.17}$$

where $n_2 = 12\pi\chi^{(3)}/n_0$. With these definitions, and assuming that the Bragg condition is nearly satisfied so that $\beta/\beta_0 \simeq 1$, Eq. (3.15) becomes

$$\partial_z^2 E + (\beta^2 + 4\beta\kappa\cos 2\beta_0 z)E = -\gamma\beta|E|^2 E \ . \tag{3.18}$$

In general, the periodic modulation of a medium will give rise to an infinite number of diffraction orders. However, in the vicinity of the Bragg frequency only two orders are phase-matched with the structure and will grow to a significant amplitude [5]. The field in the structure is thus taken as a sum of two counterpropagating waves

$$E(z) = E_F(z)e^{i\beta z} + E_B(z)e^{-i\beta z} \tag{3.19}$$

where the complex amplitudes are assumed to vary little within an optical wavelength. (This assumption has been rigorously established by Kogelnik for the periodic structure [5].) Using Eq. (3.19) in (3.18), invoking the slowly varying envelope approximation ($|d^2E/dz^2| << |\beta dE/dz|$) and comparing terms with equal exponentials we finally obtain the coupled wave equations

$$-i\partial_z E_F = \kappa E_B e^{-i2\Delta\beta z} + \gamma(|E_F|^2 + 2|E_B|^2)E_F \tag{3.20a}$$

$$i\partial_z E_B = \kappa E_F e^{i2\Delta\beta z} + \gamma(|E_B|^2 + 2|E_F|^2)E_B \tag{3.20b}$$

where $\Delta\beta = \beta - \beta_0$. In deriving the above equations we have discarded rapidly-varying terms with exponentials $\exp \pm i3\beta z$.

These are the model equations that describe wave propagation in a periodic structure with an intensity-dependent refractive index. The physical interpretation of these equations is that a wave (E_F or E_B) grows in amplitude along the propagation direction as a result of coupling (through κ) to the other wave. Simultaneously it falls out of phase synchronism with the structure as a result of the detuning $\Delta\beta$. The effect of the intensity-dependent terms is to cause an additional change in the relative phase of the two waves as they propagate. In the next section we shall obtain an exact closed-form description of the transmission character-

istics of the non-linear DFB structure.

D. Exact Solutions

The coupled-wave equations can be solved by methods used by Armstrong et al. in their analysis of harmonic generation [8]. Writing $E_F = |E_F|\exp(i\phi_F)$ and $E_B = |E_B|\exp(i\phi_B)$ in Eqs. (3.20) and equating real and imaginary parts we obtain

$$\partial_z|E_F| = \kappa|E_B|\sin\theta \tag{3.21a}$$

$$\partial_z|E_B| = \kappa|E_F|\sin\theta \tag{3.21b}$$

$$\partial_z\theta = 2\Delta\beta+3\gamma(|E_F|^2+|E_B|^2)+\kappa(|E_B|/|E_F|+|E_F|/|E_B|)\cos\theta \tag{3.21c}$$

where $\theta = 2\Delta\beta z + \phi_F - \phi_B$.

From Eqs. (3.21a) and (3.21b), we obtain

$$|E_F|\partial_z|E_F| = |E_B|\partial_z|E_B|$$

which leads to a conservation law for power flow:

$$|E_F|^2 - |E_B|^2 = |E_T|^2, \quad \text{a constant.} \tag{3.22}$$

Using (3.21a) and (3.21b), Eq. (3.21c) can be written in the form

$$-(\cot\theta)\partial_z(\ln|E_FE_B|\cos\theta) = 2\Delta\beta+3\gamma(|E_F|^2+|E_B|^2) \tag{3.23}$$

which can be integrated to yield another constant

$$\Gamma=|E_F||E_B|\cos\theta+(2\Delta\beta-3\gamma|E_T|^2)|E_F|^2/2\kappa+3\gamma|E_F|^4/2\kappa. \qquad (3.24)$$

Equations (3.24) and (3.22) are now used to eliminate $\sin\theta$ and $|E_B|$ from (3.2a) resulting in a single differential

$$|E_F|\partial_z|E_F| = \kappa\{|E_F|^2(|E_F|^2 - |E_T|^2)^2$$

$$- [\Gamma-|E_F|^2(3\gamma|E_F|^2-2\Delta\beta+3\gamma|E_T|^2)/2\kappa]^2\}^{1/2}. \qquad (3.25)$$

At the exit of the structure z = L, the backward flux $|E_B|^2$ must vanish, hence $|E_F(L)|^2 = |E_T|^2$ is the transmitted flux. This boundary condition is used to evaluate the constant Γ as

$$\Gamma = \frac{\Delta\beta|E_T|^2}{\kappa} \quad . \qquad (3.26)$$

Finally we normalize all intensities by a critical intensity

$$|E_c|^2 = 2\lambda_0/3\pi n_2 L \qquad (3.27)$$

and find that the forward flux $y = |E_F|^2/|E_c|^2$ is given by

$$(1/2\partial_\zeta y)^2 - (y-J)[(\kappa L)^2 y-(y-J)(\Delta\beta L+y)^2] = 0 \qquad (3.28)$$

where $\zeta = z/L$ and $J = |E_T|^2/|E_c|^2$.

Equation (3.28) can be recognized as the energy of a unit-mass particle moving in the quartic potential (Fig. (3.6))

$$V(y) = (J-y)\{(\kappa L)^2 y - (y-J)[\Delta\beta L+y]^2\}. \qquad (3.29)$$

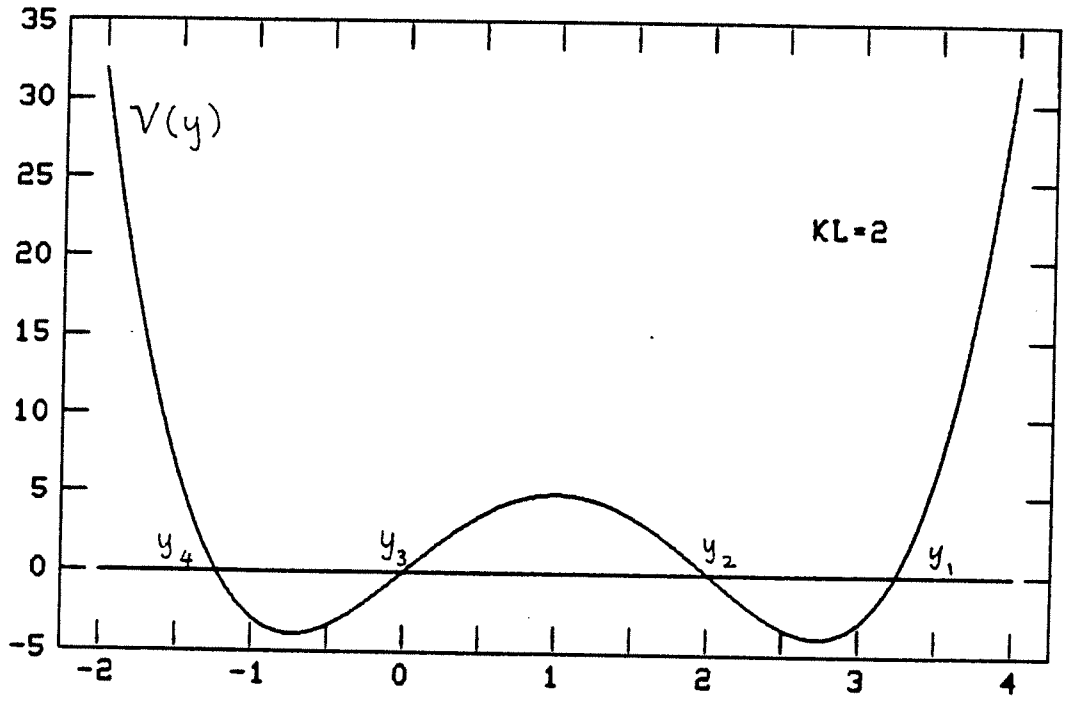

Fig. (3.6): Quartic potential for the forward flux in a nonlinear DFB structure. Here $\kappa L = 2$, $\Delta\beta L = 0$, $J = 2$.

The roots y_i (i=1 to 4) of V(y) correspond to the classical turning points of the particle and are, in general, functions of the transmitted intensity J. Since y is positive, the motion is confined to the region between y_1 and $y_2 = J$. The other roots y_3 and y_4 bound physically inaccessible regions and can be complex. (We remark that there is no apparent connection between the onset of bistability and the shape of the potential V(y).)

The solution of Eq. (3.28) can be written

$$\int_I^{y(\zeta)} \frac{dy}{[-V(y)]^{1/2}} = 2\zeta \ , \tag{3.30}$$

where I is the incident flux normalized to $|E_c|^2$. Since at the exit of the structure y(1) = J, the transmitted intensity is given implicitly by

$$\int_I^J \frac{dy}{[-V(y)]^{1/2}} = 2. \tag{3.31}$$

For further analysis, it is convenient to rewrite Eq. (3.30) so that one of the limits of the integral is a root of the quartic V(y). Here the appropriate root is Y_2=J, thus (3.30) becomes

$$\int_{y(\zeta)}^{J} \frac{dy}{[-V(y)]^{1/2}} = 2(1-\zeta). \tag{3.32}$$

Equations (3.31) and (3.32) are elliptic integrals of the first kind which can be inverted using standard techniques [9]. Details of the calculation are given in Appendix B. Here we present only the final results. From Eq. (3.31) the relation between incident (I) and transmitted (J) intensities is

$$I = y_3(J) + \frac{y_3(J) - y_2(J)}{\left[\frac{y_1(J)-y_2(J)}{y_1(J)-y_3(J)}\right] sn^2(u|m) - 1} \tag{3.33}$$

where the y_i are roots of $V(y)$. The function $sn(u|m)$ is a Jacobian elliptic function with argument

$$u = [(y_1-y_3)(y_2-y_4)]^{1/2} \tag{3.34}$$

and modulus

$$m = \frac{(y_1-y_2)(y_3-y_4)}{(y_1-y_3)(y_2-y_4)} . \tag{3.35}$$

For zero detuning ($\Delta\beta=0$), it is easy to solve for the roots of $V(y)$. These are $y_2=J$, $y_3=0$, and

$$y_1 \equiv y_+ = \frac{J}{2} + \left[\left(\frac{J}{2}\right)^2 + (\kappa L)^2\right]^{1/2} \tag{3.36}$$

$$y_4 \equiv y_- = \frac{J}{2} - \left(\left(\frac{J}{2} \right)^2 + (\kappa L)^2 \right)^{1/2} . \tag{3.37}$$

Eq. (3.33) then reduces to

$$I = \frac{J}{1 + \left(\frac{y_-}{y_+} \right) sn^2 \left(-y_+ \middle| \left(\frac{y_-}{y_+} \right)^2 \right)} . \tag{3.38}$$

The spatial distribution of the forward flux y is found from (3.32) to be

$$y(\zeta) = \frac{J}{1 + \left(\frac{y_-}{y_+} \right) sn^2 \left((\zeta - 1) y_+ \middle| \left(\frac{y_-}{y_+} \right)^2 \right)} . \tag{3.39}$$

To evaluate Eqs. (3.33) and (3.38) we start with a given value of the output J. For this value of J we find the roots $y_i(J)$ of the quartic V(y). These roots are then used in the method of Arithmetic-Geometric Mean [10] to compute the elliptic functions. The input intensity I is then found from Eq. (3.33), which for the case of zero-detuning reduces to (3.38).

Figs. (3.7) show plots of Eq. (3.38) obtained by the strategy outlined above. The different curves are for different values of the coupling constant κL. In Fig. (3.7a), $\kappa L = 1$, and the effect of feedback is negligible. In Fig. (3.7b) $\kappa L = 1.4$, and for this increased value of coupling constant the input-output curve shows a region of large differential gain. Where the curve has a steep positive

Fig. (3.7): Transmitted (J) vs. incident (I) intensity of nonlinear distributed-feedback structure for different values of coupling constant κL. (a) $\kappa L = 1$, (b) $\kappa L = 1.4$, (c) $\kappa L = 2$, (d) $\kappa L = 4$. (e) Transmission of a nonlinear Fabry-Perot with reflectivity $R = 0.5$ shown for comparison.

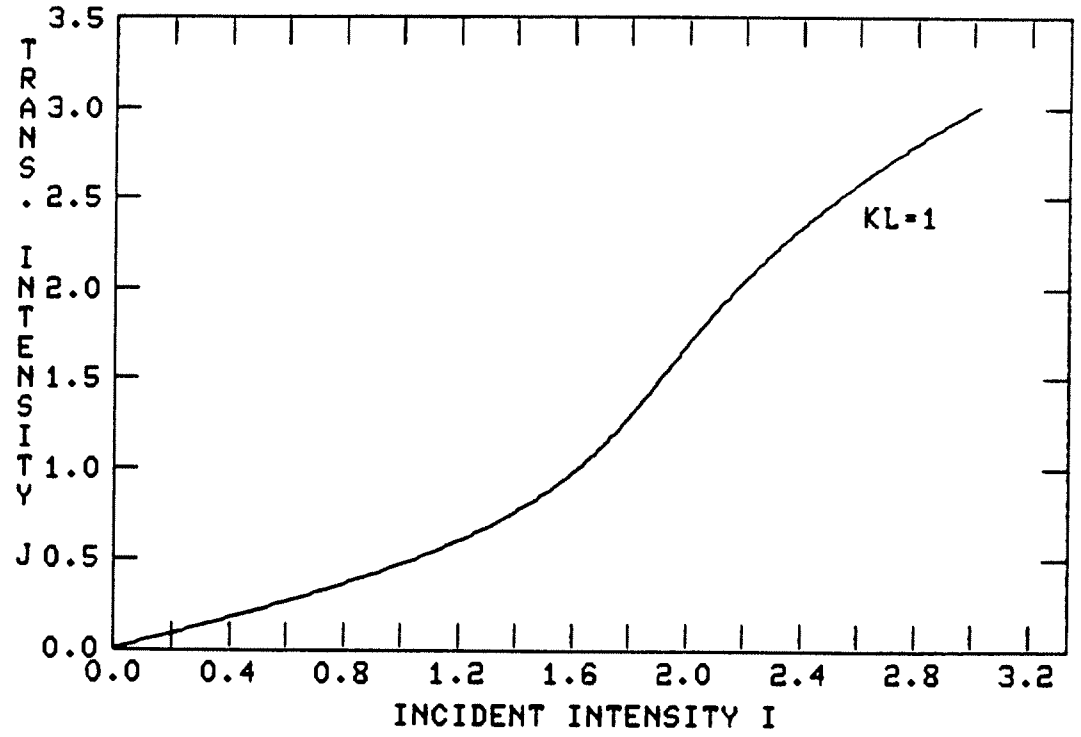

Fig. (3.7a)

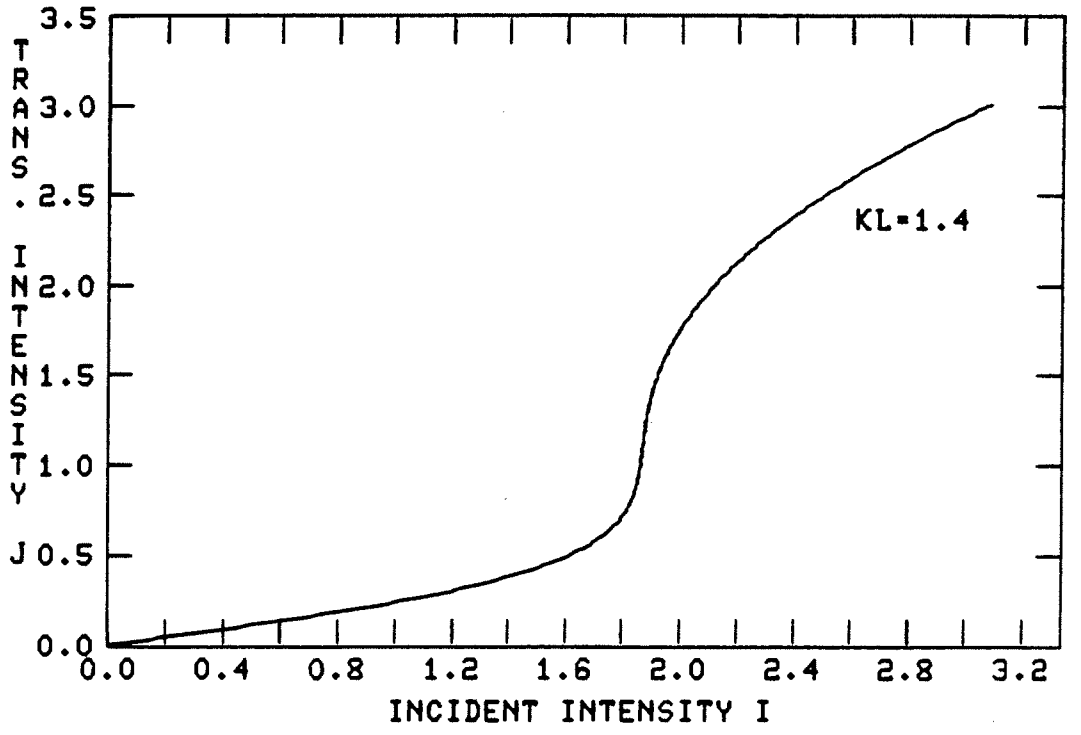

Fig. (3.7b)

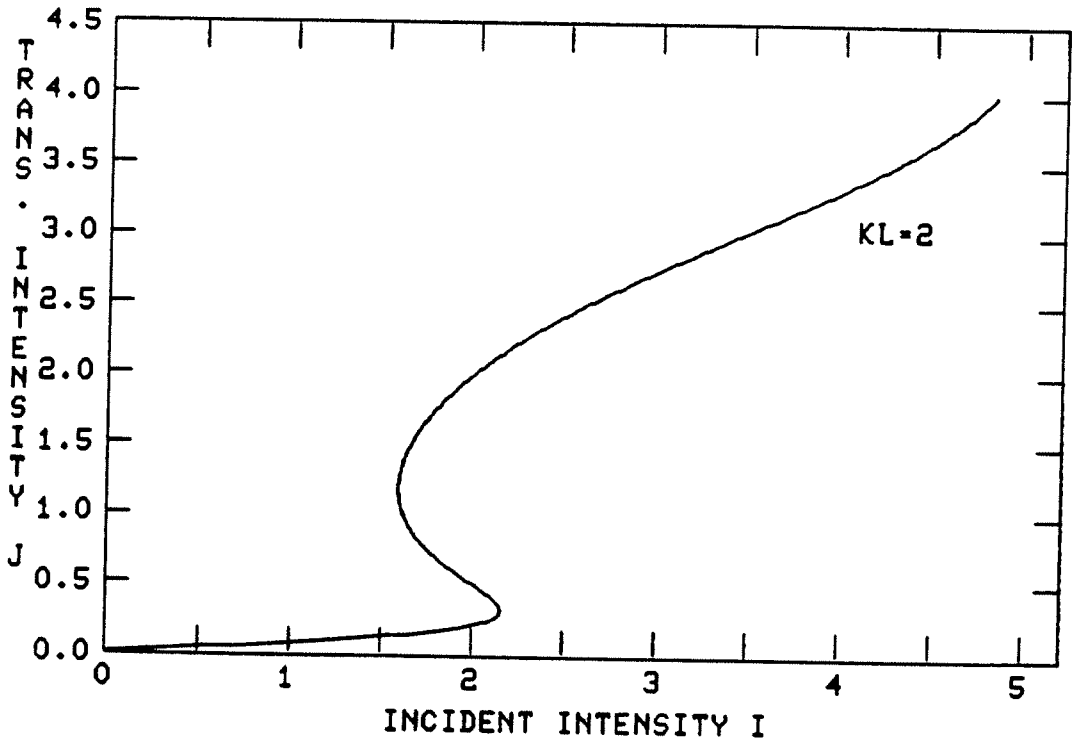

Fig. (3.7c)

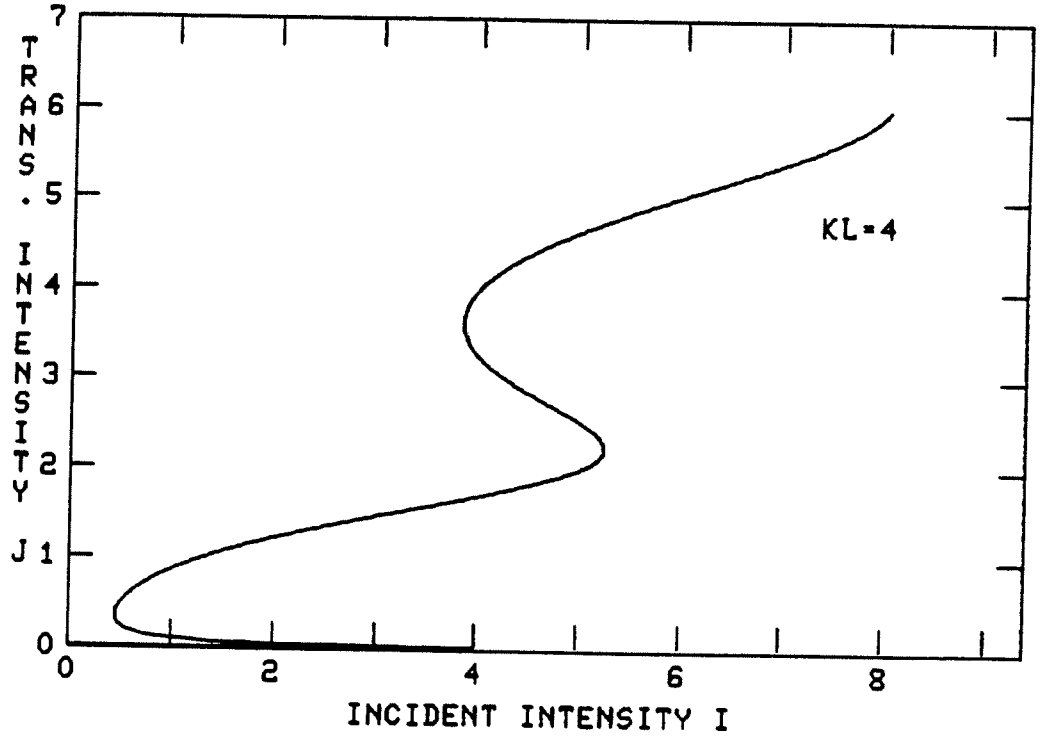

Fig. (3.7d)

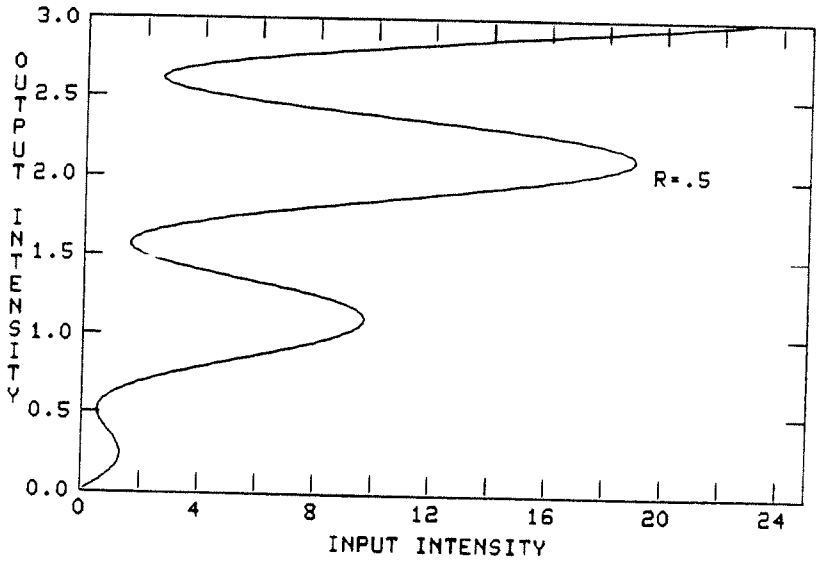
3.0
2.5
2.0
1.5
1.0
0.5
0.0
OUTPUT INTENSITY
R=.5
0
4
8
12
16
20
24
INPUT INTENSITY

Fig. (3.7e)

slope, small changes in input intensity are converted to large changes in the output. In Fig. (3.7c) κL has been increased to $\kappa L = 2$. We see that I is now a multiple-valued function J. As the input intensity is varied the output initially changes little until a critical input intensity I_c is reached. At that point the output jumps discontinuously to a higher value. When the input is now reduced the output will drop down at a different critical intensity, resulting in a hysteresis loop. In Fig. (3.7d) $\kappa L = 4$, and higher order bistable regions begin to appear. This is because the DFB transmission function begins to have strong periodic sidelobes. As the input intensity tunes through these resonances by changing the refractive index, the output jumps discontinuously as each sidelobe is crossed. For sufficiently large κL, the nonlinear DFB transmission approaches that of the Fabry-Perot which is shown for comparison in Fig. (3.7e). The behaviour of the reflected signal is shown in Figs. (3.8). Fig. (3.9) shows the effect of the detuning $\Delta\beta L$ on the switching characteristics of the DFB-BOD. These curves obtained from Eq. (3.33) show that for a given κL, the switching threshold can be reduced by operating on the high frequency side of the Bragg resonance. However, the reduction in threshold is accompanied by a decrease in hysteresis width. This is shown in Fig. (3.10) where we summarize the dependence of the width of the hysteresis zone on detuning and coupling constant.

Fig. (3.8): Reflected intensity vs. incident intensity for nonlinear DFB structure with $\kappa L = 2$. (a) $\kappa L = 2$, and (b) $\kappa L = 4$. The detuning is $\Delta\beta L = 0$.

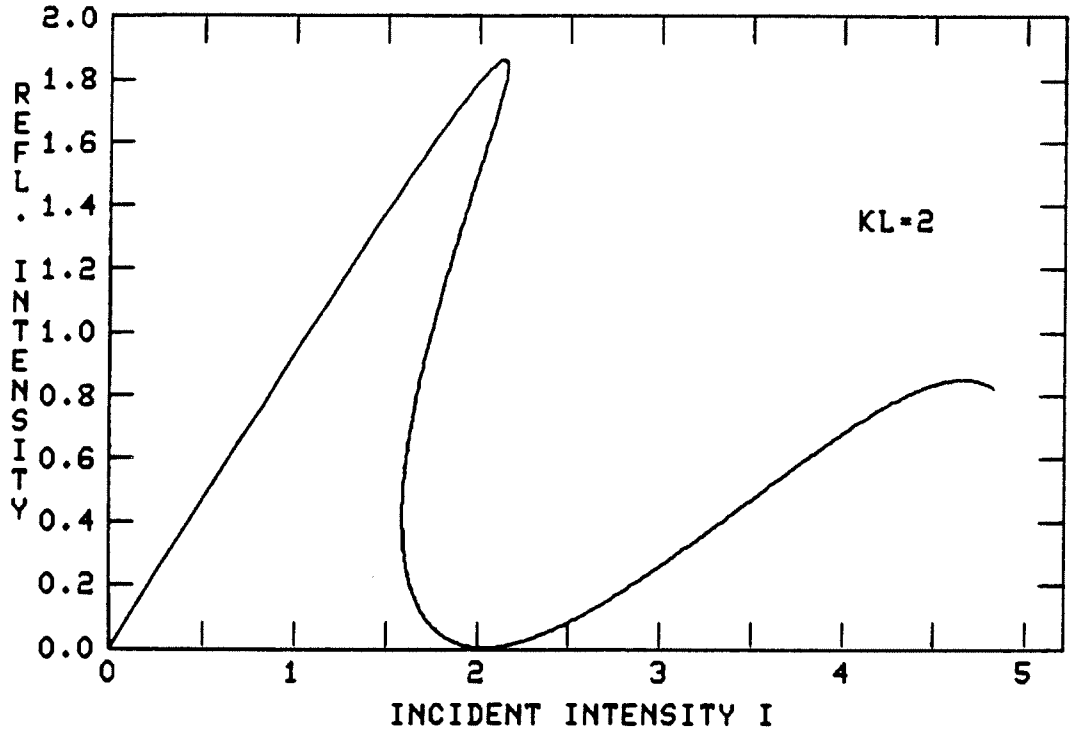

Fig. (3.8a)

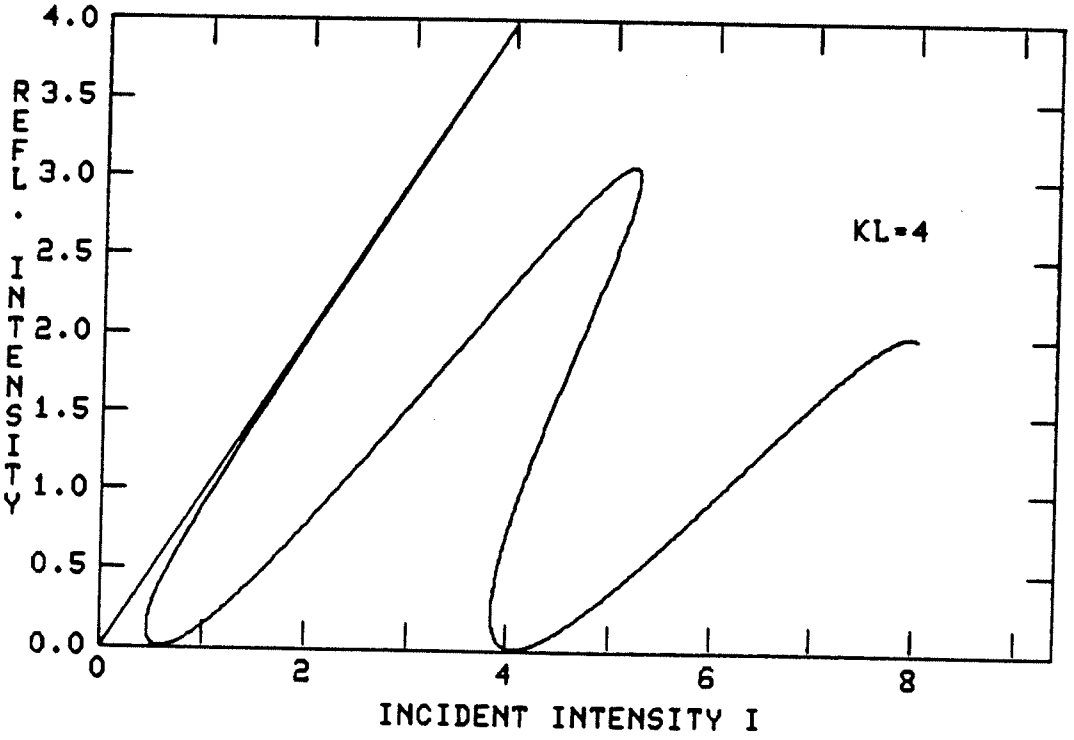

Fig. (3.8b)

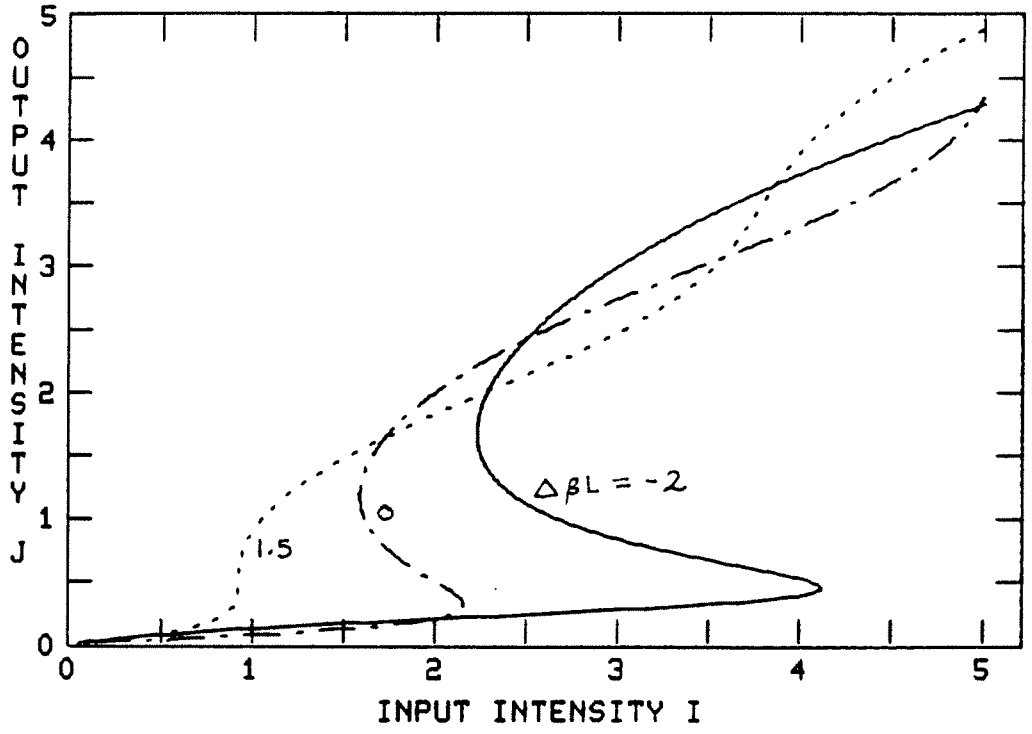

Fig. (3.9): Transmitted (J) vs. incident (I) intensity for a nonlinear DFB structure with $\kappa L = 2$ for different values of detuning $\Delta\beta L$.

Fig. (3.10): Dependence of width of the hysteresis zone on detuning and coupling constant. The switch-on intensity is given approximately by $I_s \simeq \kappa L - \Delta\beta L$.

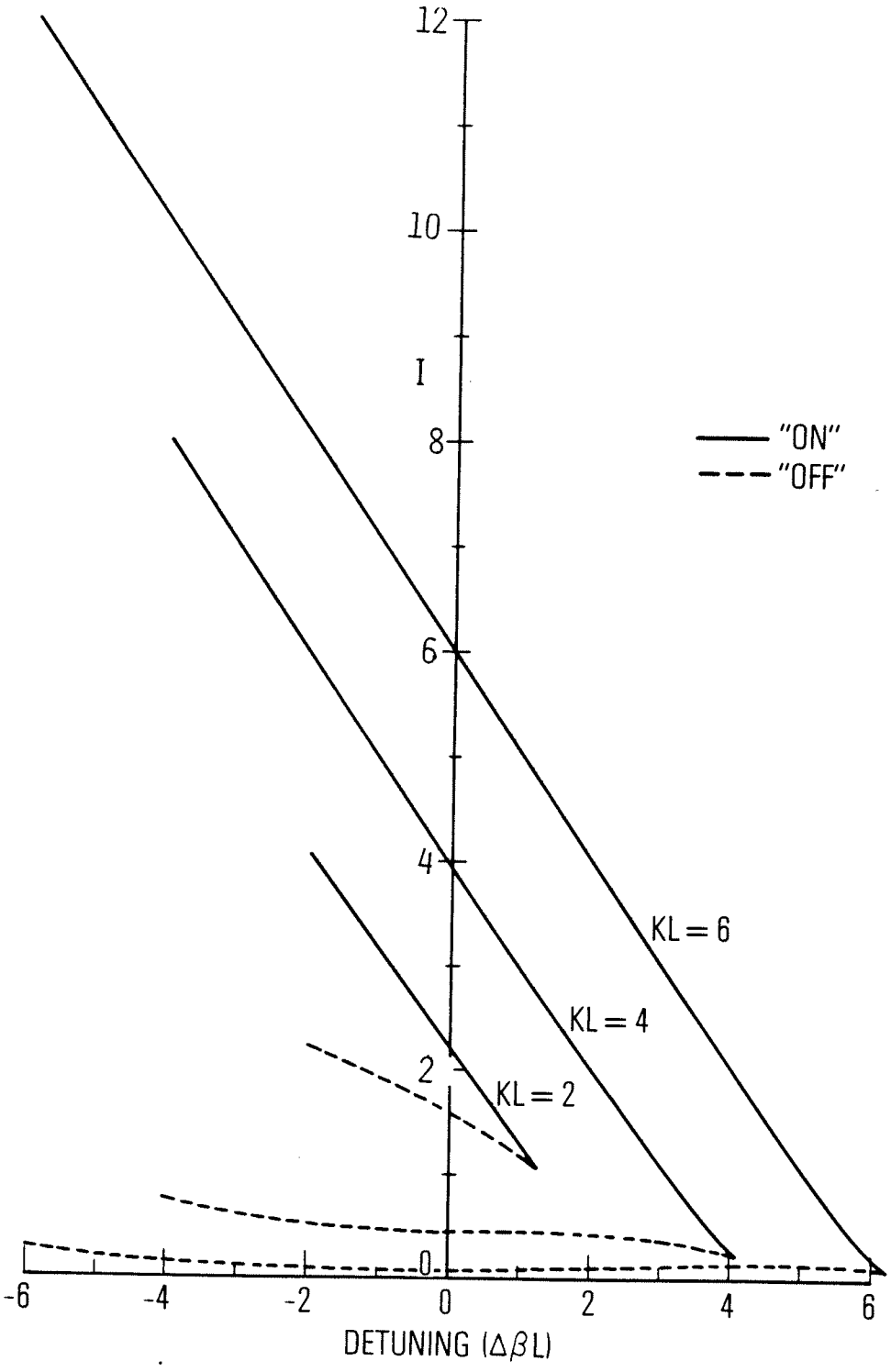
12
10
I
8
6
4
2
0
"ON"
"OFF"
KL = 6
KL = 4
KL = 2
-6
-4
-2
0
2
4
6
DETUNING (ΔβL)

The bistability discussed here is a manifestation of the fact that for the same input intensity there are three possible spatial intensity distributions that satisfy equations (3.20) and the associated boundary conditions. By analogy with the nonlinear Fabry-Perot, we conjecture that one of these spatial distributions is unstable and is thus physically inaccessible in steady state. Fig. (3.11) shows the spatial intensity distributions that correspond to the same input intensity. The distributions A and C correspond to the stable regions of the transmission curve while B is unstable in steady state.

E. Approximate Results

The exact solutions presented in the previous section provide a complete steady state description of the behavior of a lossless nonlinear DFB structure. However, because of the complexity of the elliptic functions involved, it is difficult to obtain from these solutions useful analytic expressions for key quantities such as the critical switching intensity in terms of device parameters. In this section we present some simple approximate formulas which yield a great deal of physical insight into the operation of a DFB-BOD. These results are valid in the limit of high coupling constant ($\kappa L > 2$) and small detuning ($\Delta\beta L < \kappa L$).

To obtain the approximate results, we study the exact solutions as represented in Fig. (3.10). We find that for

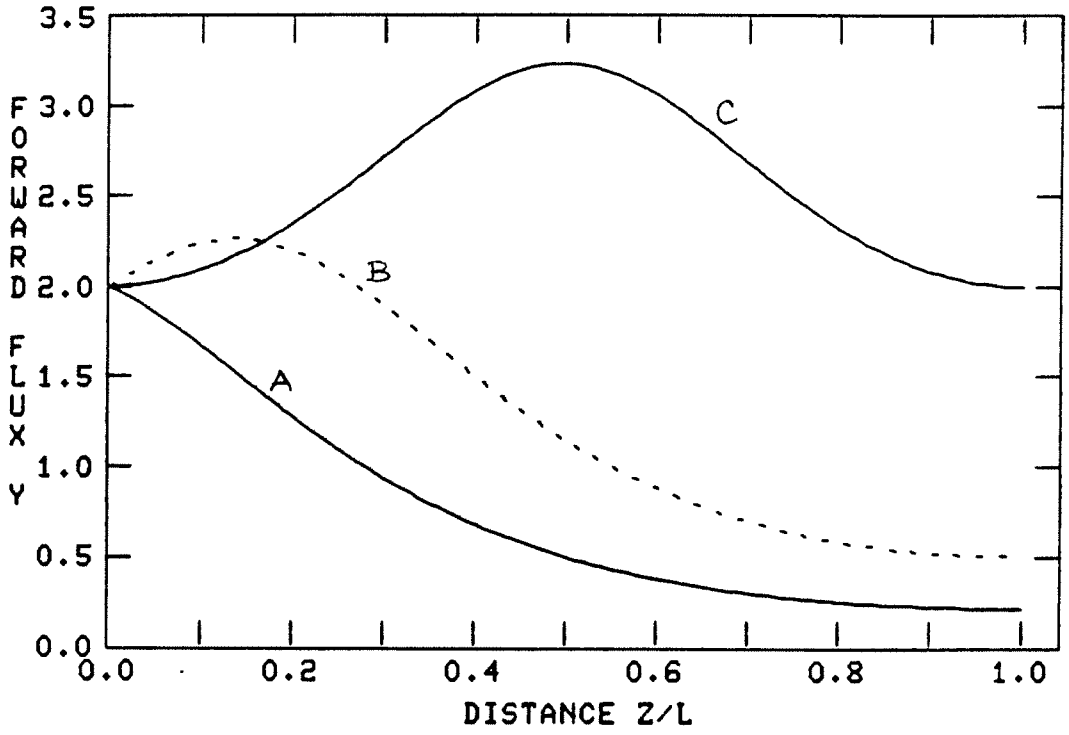

Fig. (3.11): The three spatial distributions of forward flux that correspond to the same input intensity I = 2. Distribution B is probably unstable.

a given coupling constant κL, the switching intensity decreases linearly with increasing detuning, $\Delta\beta L$. Also, for a fixed detuning the switching intensity increases linearly with coupling constant. We can express these trends quantitatively by writing

$$I_s \simeq \kappa L - \Delta\beta L \tag{3.40}$$

where I_s is the normalized switching intensity. For $\kappa L > 3$ the intensity predicted by this formula is indistinguishable from that obtained numerically from the exact solution. Recalling that the dimensionless intensities are normalized by

$$|E_c|^2 = \frac{2\lambda}{3\pi n_2 L} \tag{3.41}$$

we find the switching intensity in esu is

$$|E_s|^2 \simeq \frac{2\lambda(\kappa L - \Delta\beta L)}{3\pi n_2 L} \ . \tag{3.42}$$

An interesting feature of this relation is that the switching intensity is independent of the length of the periodic structure (for $\kappa L > 2$). This is in marked contrast to the behavior of a nonlinear Fabry-Perot where an increase in the length of the medium leads to a decrease in the required switching intensity. The difference is due to the fact that in a periodic structure with large coupling ($\kappa L > 2$), the internal field drops off almost exponentially along the z-

direction. Thus most of the light is reflected in the first few periods of the structure and is unable to take advantage of the increased length of non-linear medium. In a lossless Fabry-Perot on the other hand the field is uniform throughout the medium and the nonlinear interaction occurs along the whole length of the cavity.

We now restrict attention to the case of zero detuning ($\Delta\beta L = 0$) and write $\kappa = \pi n_1/\lambda$ in Eq. (3.42) so that

$$|E_s|^2 = \frac{2}{3}\frac{n_1}{n_2} \quad . \tag{3.43}$$

From this expression we see that switch-on of the DFB-BOD occurs when the field-induced change in refractive index ($\Delta n = \frac{1}{2}n_2|E_s|^2$) balances out the built-in periodic perturbation in index, n_1.

The index change at the threshold for bistability is thus

$$\Delta n_c = \frac{1}{3}n_1 \quad . \tag{3.44}$$

F. Practical Considerations

In this section we study the feasibility of an operating DFB-BOD that uses currently available materials and techniques. We also point out effects neglected in the theory but which have to be considered in a practical device.

1. Design Considerations

Ideally, the materials used for bistable devices should be solid state and have high nonlinear indices, low losses and be available with good optical quality. Currently the two most promising materials for device applications are the semiconductors GaAs and InSb. For the purposes of making numerical estimates we will focus on InSb which has a third order susceptibility $\chi^{(3)}$ on the order of 10^{-2} esu at 5°K, at a wavelength of 5.3μ (the wavelength of the CO laser) [11]. A waveguide structure may be made out of this medium by epitaxial growth of a related alloy with closely matching lattice constant, such as InAsSb. (Abrokwah has discussed techniques for the liquid phase epitaxy of InSb and InAsSb in his dissertation [12].) The refractive index of InAsSb is on the order of 1% less than that of InSb and can be varied by changing the composition of the alloy system. We choose the thickness of the guiding layer to be W = 2.6μ. To create the surface corrugations, a mask is first made by exposing a layer of photoresist to the interference pattern produced by two argon laser beams, for example. The grating periodicity is given by

$$\Lambda = \lambda/2\sin\theta$$

where λ is the wavelength of the argon laser (λ = 0.4579) and θ is the interference angle. Taking into account the high linear refractive index of In Sb (~3.75), the required

grating periodicity for operation at 5.3μ is on the order of 0.7μ, which is easy to create. The grating is then transferred onto the surface of the waveguide by ion milling through the photoresist mask, or by chemical etching. We will assume a groove depth of 0.3μ.

For a TE mode the coupling constant is given by [13]

$$\kappa = \frac{\pi h}{\lambda} \frac{n_f^2 - n_e^2}{2Wn_e} \tag{3.45}$$

where h is the peak-to-peak perturbation height, W is the thickness of the guiding layer, n_f is the film index and n_e is the effective index of the unperturbed mode. For reference we list below the parameters of our corrugated waveguide:

$$h = 0.3\mu$$
$$W = 2.6\mu$$
$$n_f(\text{InSb}) = 3.75$$
$$n_s(\text{InAsSb}) = 3.56$$
$$n_e = 3.6$$
$$n_2 = 10^{-1} \text{ esu} .$$

The effective index n_e has a value between n_s and n_f and can be determined from waveguide measurements [13]. Using this data we obtain a coupling constant of $\kappa = 100\text{cm}^{-1}$. For a grating of length 5mm we therefore have

$$\kappa L = 5 .$$

Ignoring losses for the moment we find a switching intensity

$$|E_s|^2 = \frac{2\lambda\kappa}{3\pi n_2} = 0.112 \text{ esu}$$

which is equivalent to $100 W/cm^2$. This implies that if we focus the input beam down to a spot size of diameter 10μ we only require a switching power of $80\mu W$.

The loss due to absorption in InSb is a maximum of $1cm^{-1}$ at the operating wavelength of 5.3μ. Suppose scattering losses increase the total loss to $2cm^{-1}$. Then $\alpha L = 0.2$, which does not change the bistable transfer curve by much. As we will see in the next section a loss of 0.2 only increases the switching threshold by about 10%.

2. Effect of Nonlinear Waveguiding

In the proposed waveguide geometry for the distributed feedback BOD, the guiding layer consists of a medium whose refractive index is intensity-dependent. The mode properties of this waveguide will therefore change as one varies the intensity of the incident wave. It is therefore necessary to consider how this nonlinear waveguiding will affect the properties of the DFB-BOD.

The analysis of this chapter has assumed for simplicity a single-mode propagating in the guide. We can make the reasonable assumption that if the refractive index of the guiding film does not change sufficiently (under the action of the beam intensity) to bring in other guided modes, the

properties of the waveguide will not change much. To quantify this, consider the approximate formula for the number of guided modes in the waveguide [6]

$$N = \frac{2W}{\lambda}(n_f^2 - n_s^2)^{1/2}, \tag{3.46}$$

where n_f is the refractive index of the guiding film, n_s is that of the substrate W is the film thickness, and λ is the free space wavelength of the incident light. To account for the intensity-dependent film index we write

$$n_f = n_{fo} + \Delta_n$$

where $\Delta n = \frac{1}{2}n_2|E|^2$. We will find the size of Δn required to change the number of guided modes from N = 1 to N = 2 and compare that to the field induced Δn at the threshold for bistability.

Setting $W = \lambda/2$ we find from Eq. (3.46) that

$$\Delta n \simeq \frac{0.75}{2n_{f_0}}$$

is the index change required to introduce another guided mode. In the previous section we showed that the index change at threshold is given by

$$\Delta n_c = \frac{\kappa\lambda}{3\pi} .$$

For our InSb device with $\kappa L = 5$ and $n_{f_0} = 3.6$ at $\lambda = 5.3\mu$,

we find

$$\Delta n_c \sim .003$$

which is more than 2 orders of magnitude less than the $\Delta n = 0.1$ required to change the mode properties of the guide. Thus the effect of nonlinear waveguiding can be neglected in practical DFB-BODs.

3. Effects of Loss, Chirp and Taper

So far we have assumed that there are no losses within the DFB structure and that the grating has perfect periodicity. In practice waveguides with corrugated surfaces are notoriously lossy and often have a z-dependent period and amplitude introduced inadvertently in the fabrication process [13]. These variations, konwn as chirp and taper respectively, may also be created by design in order to produce a filter with a certain desired response [14]. In this section we show that the theory of the nonlinear DFB can be generalized in a straightforward manner to include these effects.

A slow variation in the amplitude and phase of the sinusoidal grating can be incorporated by defining a z-dependent complex coupling constant

$$K(z) = \kappa(z)e^{i\phi(z)}.$$

$\kappa(z)$ is then the taper function and $\phi(z)$ is the chirp.

With loss, chirp and taper, the coupled-wave equations now become

$$\partial_z E_F = i\kappa(z) E_B e^{-i(2\Delta\beta z - \phi(z))} + i\gamma(|E_F|^2 + 2|E_B|^2)E_F - \frac{1}{2}\alpha E_F \qquad (3.47a)$$

$$\partial_z E_B = -i\kappa(z) E_F(z) e^{i(2\Delta\beta z + \phi(z))} - i\gamma(|E_B|^2 + 2|E_F|^2)E_B + \frac{1}{2}\alpha E_B \qquad (3.47b)$$

where α is the absorption coefficient. Exact closed form solutions to these equations have not been found. We have therefore used a fourth-order Runge-Kutta scheme to solve them numerically for different values of loss and various chirp and taper functions. Some representative solutions are presented here.

Fig. (3.12) shows the effect of loss on a DFB BOD with coupling constant $\kappa L = 2$ and zero-detuning. We see, as expected, that the presence of loss increases the required switching intensity, narrows the width of the hysteresis loop and decreases the jump between the low and high output states. When loss is sufficiently high, it will of course destroy the bistability features as shown in Fig. (3.12).

Sample calculations of the effects of chirp and taper are shown in Figs. (3.13) and (3.14). The taper function is taken as

$$\kappa = \kappa_0 (1 + T\frac{z}{L})$$

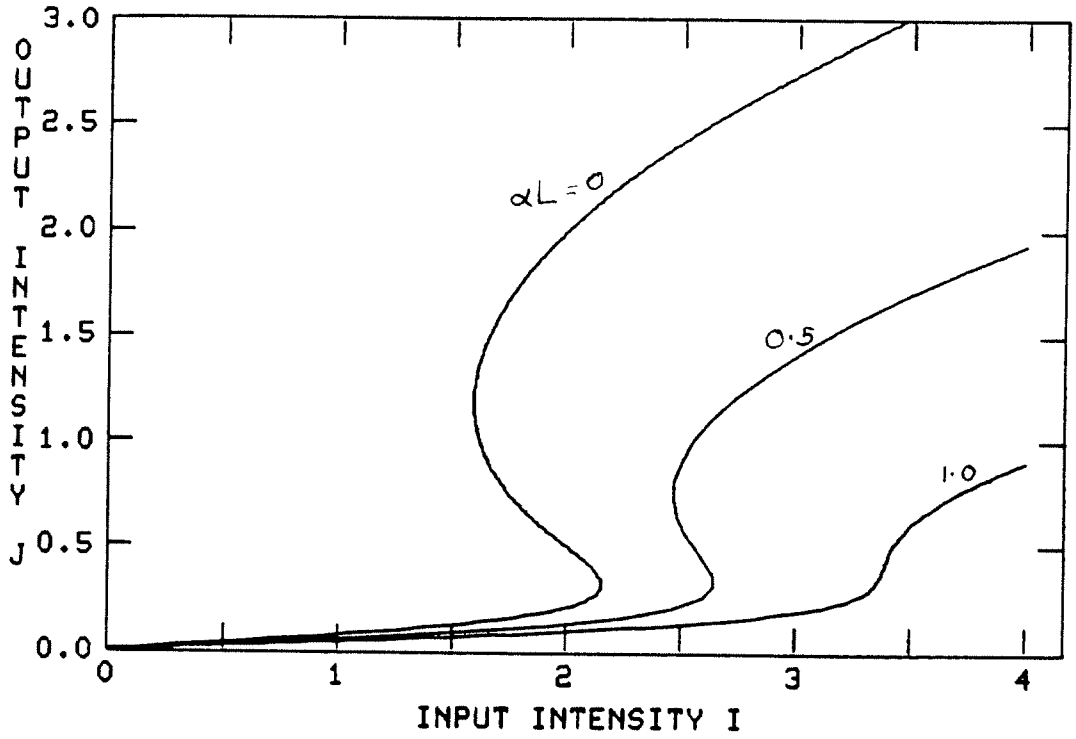

Fig. (3.12): Effect of loss on a DFB bistable optical device. Here $\kappa L = 2$ and $\Delta\beta L = 0$.

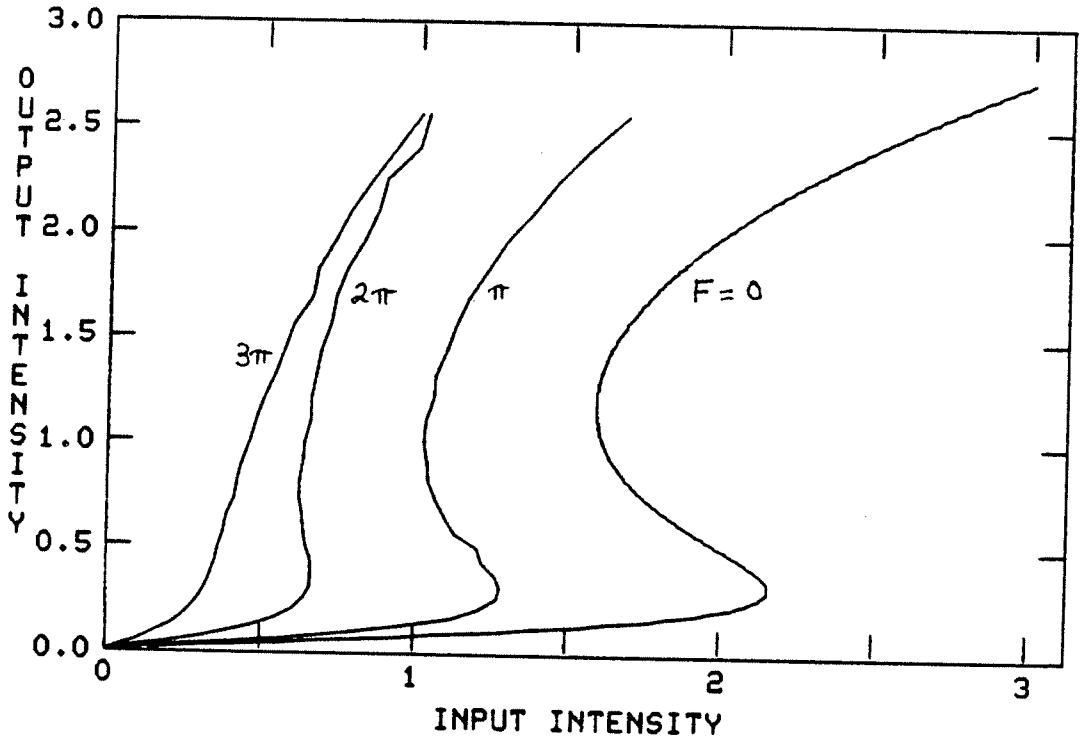

Fig. (3.13): Effect of a frequency chirp on a DFB bistable optical device. The chirp acts as an extra detuning added on to $\Delta\beta L$.

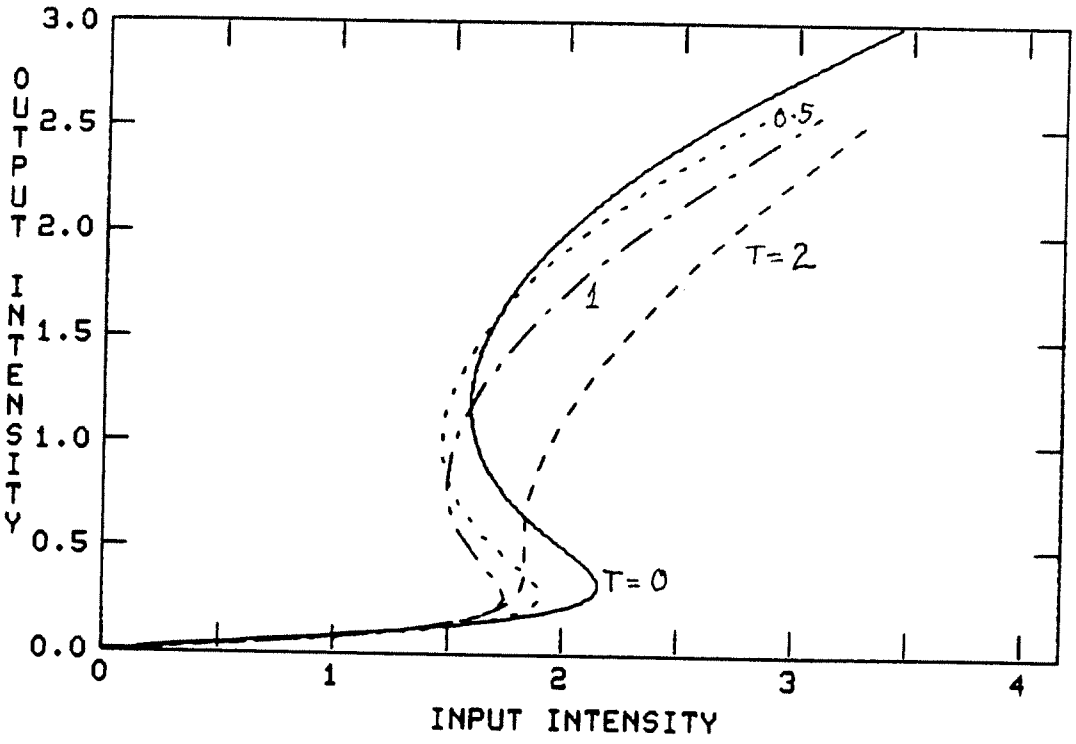

Fig. (3.14): Effect of a linear taper on a DFB bistable optical device with $\kappa L = 2$ and $\Delta\beta L = 0$.

and the chirp is described by

$$\phi(z) = F\frac{z^2}{L^2}$$

where T and F are constants.

4. Effect of a Saturable Nonlinear Index

In our analyses we have only considered the lowest order term in the nonlinear polarization that leads to an intensity-dependent refractive index. This term, cubic in the electric fields, is the dominant one in media with a center of inversion symmetry. At sufficiently high intensities, however, higher-order terms become important and these generally tend to reduce the size of the nonlinear index. Thus when one writes the refractive index as

$$n = n_0 + n_2 I$$

the nonlinear index n_2 is no longer constant but is a decreasing function of the intensity I. This effect, known as saturation, has important observable consequences for the operation of bistable optical devices. For example, in a recent experiment using the semiconductor GaAs [15], saturation of the nonlinear index made it impossible to observe bistability beyond the first Fabry-Perot order. More recently, under different experimental conditions, Miller et al. [11] have observed fifth-order bistability in InSb. Here

too saturation manifested itself in that each successive Fabry-Perot order required a successively greater incremental change in input intensity.

When saturation is included, the nonlinear DFB equations can no longer be integrated analytically. Their numerical integration however is straightforward and the results are presented here.

In our simulations we consider a saturable index of the form

$$n_2 = \frac{n_{20}}{1 + I/I_s}$$

where I_s is the saturation intensity. The presence of saturation increases the switching intensity and may even eliminate bistability completely (Fig. (3.15)). From several computer runs, a rule of thumb emerges: that in order to observe bistability the normalized saturation intensity should be at least three times the coupling constant κL, i.e.,

$$I_s \geq 3\kappa L.$$

G. Conclusions

We have shown that a distributed feedback structure with an intensity-dependent refractive index displays hysteresis and bistability. Such structures provide a useful alternative to the Fabry-Perot device especially in planar

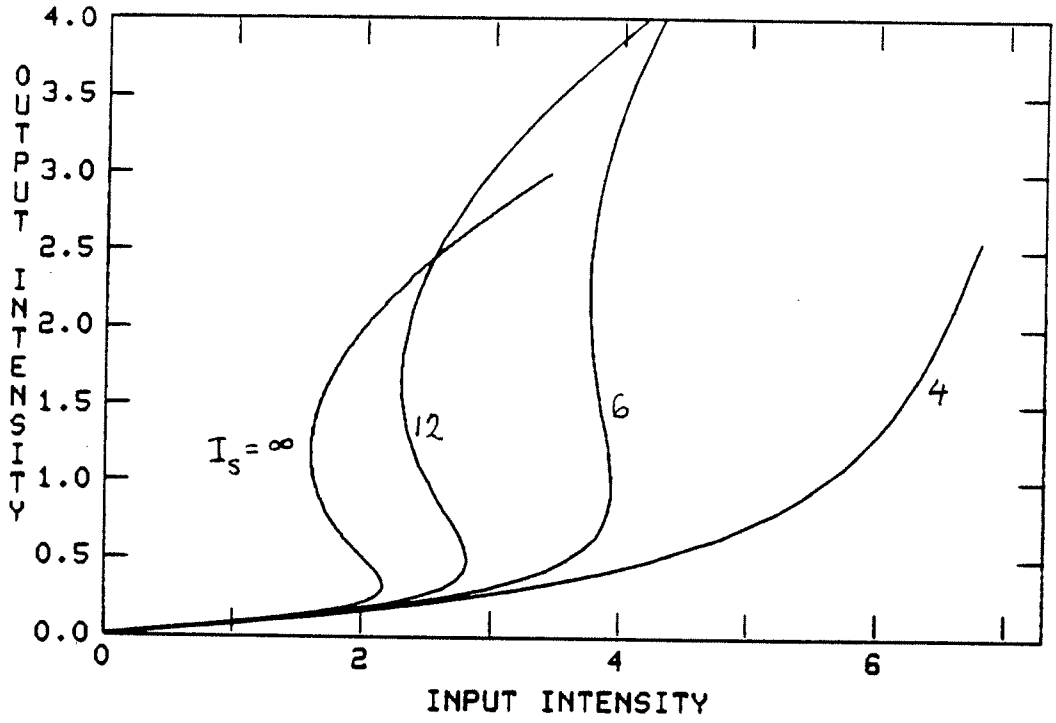

Fig. (3.15): Effect of a saturable nonlinear index on a DFB bistable optical device.

integrated-optics configurations.

The analysis presented in this chaper assumed that there are no Fresnel reflections at the ends of the DFB structure and that the backward wave grows from zero amplitude at the exit. For high index materials like InSb this assumption is clearly quite questionable since the Fresnel reflection in this case exceeds 30%. While end reflections may be reduced by applying antireflection coatings or slanting the ends at Brewster's angle, they can never be eliminated entirely and their effect should be considered in any real situation. Since the extra Fabry-Perot effect due to end reflections will tend to increase the cavity fields they may result in a net decrease in the required switching intensities. A quantitative analysis of this effect remains to be done.

REFERENCES -- CHAPTER III

1. A. Yariv and M. Nakamura, "Periodic structures for integrated optics," IEEE J. Quantum Electron., vol. QE-13, p. 233, 1977.

2. M. Okuda and K. Onaka, "Bistability of optical resonator with distributed Bragg-reflectors by using the Kerr effect," Jpn. J. Appl. Phys., vol. 16, p. 769, 1977.

   M. Okuda, M. Toyota, and K. Onaka, "Saturable optical resonators with distributed Bragg-reflectors," Opt. Commun., vol. 19, p. 138, 1976.

3. H.G. Winful, J.H. Marburger, and E. Garmire, "Theory of bistability in nonlinear distributed-feedback structures," Appl. Phys. Lett., vol. 35, p. 379, 1979.

4. H.A. Haus, "Gain saturation in distributed feedback lasers," Appl. Optics, vol. 14, p. 2650, 1976.

5. H. Kogelnik, "Coupled wave theory for thick hologram gratings," Bell System Tech. J., vol. 48, p. 2909, 1969.

   H. Kogelnik and C.V. Shank, "Coupled-wave theory of distributed feedback lasers," J. Appl. Phys., vol. 43, p. 2327, 1971.

6. H. Kogelnik, in Integrated Optics. T. Tamir, ed. Berlin: Springer-Verlag, 1974.

7. P.D. Maker and R.W. Terhune, "Study of optical effects due to an induced polarization third order in the electric field strength," Phys. Rev., vol. 137, p. A801, 1965.

8. J.A. Armstrong, N. Bloembergen, J. Ducuing, and P.S. Pershan, "Interactions between light waves in a nonlinear dielectric," Phys. Rev., vol. 127, p. 1918, 1962.

9. P.F. Byrd and M.D. Friedman, Handbook of Elliptic Integrals for Engineers and Scientists. New York: Springer-Verlag, 1971.

10. M. Abramowitz and I. Stegon, Handbook of Mathematical Functions. National Bureau of Standards, Handbook 55, Washington, DC: U.S. Government Printing Office, 1964.

11. D.A.B. Miller and S.D. Smith, "Two-beam optical signal amplification and bistability in InSb," Opt. Commun., vol. 31, p. 101, 1979.

12. J.K. Abrokwah, unpublished Ph.D. dissertation, University of Southern California, 1979.

13. D.C. Flanders, H. Kogelnik, R.V. Schmidt, and C.V. Shank, "Grating filters for thin film optical waveguides," Appl. Phys. Lett., vol. 24, p. 194, 1974.

14. H. Kogelnik, "Filter response of nonuniform almost-periodic structures," Bell Syst. Tech. J., vol. 55, p. 109, 1976.

15. H.M. Gibbs, S.L. McCall, T.N.C. Venkatesan, A.C. Gossard, A. Passner, and U. Wiegman, "Optical bistability in semiconductors," Appl. Phys. Lett., vol. 35, p. 451, 1979.